Electronic Supplementary Information

An erbium phosphonate in pseudo-D_{5h} symmetry exhibiting field-tunable magnetic relaxation and optical correlation

Min Ren,[a] Song-Song Bao,[a]   Rute A. S. Ferreira,[b] Li-Min Zheng,[*a] Luis D. Carlos[*b]

[a] State Key Laboratory of Coordination Chemistry, School of Chemistry and Chemical Engineering,

Nanjing University, Nanjing 210093, P. R. China

[b] Physics Department, CICECO, University of Aveiro, 3810-193, Aveiro, Portugal

EXPERIMENTAL SECTION

General considerations. The ligand 1,4,7-triazacyclononane-1,4,7-triyl-tris(methylenephosphonic acid) (notpH$_6$) was prepared according to literature methods.[1] All the other starting materials were of reagent grade quality and were obtained from commercial sources without further purification. The synthesis of compounds **1**-**2** refers to the previously reported methods.[2] Elemental analysis for C, H and N were carried out on a PE 240C analyzer. IR spectra were recorded with a TENSOR 27 Fourier transform infrared spectrophotometer. Thermal analyses were performed in nitrogen on a METTLER TOLEDO TGA instrument. Powder X-ray diffraction (PXRD) data were collected in a Bruker D8 advance diffractometer. The magnetic susceptibility data were obtained on polycrystalline or powder samples using a Quantum Design SQUID VSM system. The data were corrected for diamagnetic contributions of both the sample holder and the compound obtained from Pascal's constants.[3] The photoluminescence spectra in the near-IR spectral ranges was recorded on a Bruker RFS100/S FT spectrometer (Nd:YAG laser excitation, 1064 nm).

Preparation of [Er(notpH$_4$)(H$_2$O)]ClO$_4$·3H$_2$O (1). Er(OAc)$_3$·6H$_2$O (0.05 mmol, 0.024 g) was added to a solution of notpH$_6$ (0.05 mmol, 0.020 g) in water (10 mL). HClO$_4$ (70%) was dropped into the mixture until pH = 1.0. The clear solution was left at room temperature for 2 weeks to afford colorless prismatic crystals in a yield of 35%. IR (KBr, cm^{-1}): 3442-2877 (br), 1633 (m), 1497(w) 1471(w), 1439 (w), 1155 (s), 1084 (s), 932 (m) , 769 (m), 742 (w), 623(m), 569(m); elemental analysis calcd (%) for C$_9$H$_{24}$N$_3$P$_3$O$_{14}$ClEr·3H$_2$O: C 14.45, H 4.04, N 5.62; found: C 13.83, H 3.60, N 5.40. Thermal analysis shows that in the 25-100 °C temperature range complex **1** loses 3.68 molecular water, in agreement with one coordinated water and three crystal water in single crystal structure..

Preparation of [Y(notpH$_4$)(H$_2$O)]ClO$_4$·3H$_2$O (2). The preparation of this compound follows the same procedure as for **1** except that Y(OAc)$_3$·6H$_2$O (0.05 mmol, 0.015 g) was used as the starting material instead of Er(OAc)$_3$·6H$_2$O. The clear

solution was left at room temperature for 2 weeks to afford colorless prismatic crystals in a yield of 47% based on notpH$_6$. IR (KBr, cm^{-1}): 3444-2874 (br), 1634 (m), 1494 (w), 1463(w), 1430 (w), 1155 (s), 1084 (s), 930 (m) , 773 (m), 738 (w), 623(m); elemental analysis calcd (%) for C$_9$H$_{24}$N$_3$P$_3$O$_{14}$ClY·3H$_2$O: C 16.14, H 4.52, N 6.28; found: C 16.27, H 4.23, N 6.22. Thermal analysis shows that in the 25-100 °C temperature range complex **2** loses 3.91 molecular water, in agreement with one coordinated water and three crystal water in single crystal structure.

Preparation of the 9.8 % [Er(notpH$_4$)(H$_2$O)]ClO$_4$·3H$_2$O in [Y(notpH$_4$)(H$_2$O)]ClO$_4$·3H$_2$O (1a). A mixture of Er(OAc)$_3$·6H$_2$O (0.02 mmol, 0.09 g) and Y(OAc)$_3$·6H$_2$O (0.24 mmol, 0.072 g) was added to the solution of notpH$_6$ (0.20 mmol, 0.082 g) in water (10 mL). HClO$_4$ (70%) was dropped into the mixture until pH = 1.0. The clear solution was left at room temperature for 2 weeks to afford colorless prismatic crystals in a yield of 72% based on notpH$_6$. IR (KBr, cm^{-1}): 3457-2874 (br), 1620 (m), 1450(w), 1172 (s), 1095 (s), 929 (m) , 771 (m), 741 (w), 625(m), 560(m), 463(m); elemental analysis calcd (%) for C$_9$H$_{24}$N$_3$P$_3$O$_{14}$ClEr$_{0.098}$Y$_{0.902}$·3H$_2$O: C 15.96, H 4.46, N 6.20; found: C 15.50, H 4.05, N 5.76. The amount of Er^{III} in **1a** (9.8 %) is confirmed by the inductively coupled plasma (ICP) measurements.

Crystallographic analyses: Data collection was carried out on a Bruker SMART APEXII CCD diffractometer (for **1**) and Bruker SMART APEX Duo CCD diffractometer (for **2**) equipped with graphite monochromated MoKα (λ = 0.71073 Å) radiation at 293 K (for **1**) and 296 K (for **2**). The data were integrated using the Siemens SAINT program,[4] with the intensities corrected for Lorentz factor, polarization, air absorption, and absorption due to variation in the path length through the detector faceplate. Empirical absorption and extinction corrections were applied. The structure was solved by direct method and refined on F^2 by full-matrix least squares using SHELXTL.[5] All the non-hydrogen atoms were refined anisotropically. All the hydrogen atoms were put in calculated positions or located from the Fourier maps and refined isotropically with the isotropic vibration parameters related to the non-hydrogen atom to which they are bonded.

The dc magnetic data fitting by the Condon Package

The Hamiltonian can be expressed as Eq (S1):[6]

$$\hat{H} = \hat{H}_0 + \hat{H}_{ee} + \hat{H}_{SO} + \hat{H}_{CF} + \hat{H}_M \qquad (S1)$$

where **H$_0$, H$_{ee}$, H$_{SO}$, H$_{CF}$** and **H$_M$** account for the Hamiltonians of zero level energy, interelectronic repulsion, spin-orbit effect, CF effect and Zeeman effect. The CF operator of f electrons reads, omitting B_0^0, is:[7]

$$\hat{H}_{CF} = \sum_{k=2,4}^{6} \left[B_0^k \hat{C}_0^K(i) + \sum_{q=2,3,4,6}^{k} \left(B_q^k \left[\hat{C}_{-q}^k(i) + (-1)^q \hat{C}_q^k(i) \right] \right) \right] \qquad (S2)$$

In D_{5h} symmetry approximation, only the B_0^2, B_0^4, B_0^6 CF parameters have nonzero values. The CF Hamiltonian can be expressed as:

$$\hat{H}_{CF} = \sum_{K=2,4}^{6} B_0^k \hat{C}_0^K(i) \qquad (S3)$$

The data of dc magnetic susceptibilities measured at 1 kOe were well fitted from 300 K to 10 K with a set of CF parameters (see Table S5); the electronic fine structure was obtained for the certain CF parameters (see Table S6).

The Cole-Cole plots fitting

The ac magnetic susceptibilities can be described by the Cole-Cole plots using the generalized Debye model in Eq(S4), Eq(S5)[8] (single relaxation model) and/or a linear combination of two modified Debye models, as shown in Eq(S6), Eq(S7)[9] (double relaxation model):

$$\chi'(\omega) = \chi_S + \frac{(\chi_T - \chi_S)\left[1 + (\omega\tau)^{1-\alpha} \sin(\pi\alpha/2)\right]}{1 + 2(\omega\tau)^{1-\alpha} \sin(\pi\alpha/2) + (\omega\tau)^{2(1-\alpha)}} \qquad (S4)$$

$$\chi''(\omega) = \frac{(\chi_T - \chi_S)\left[1 + (\omega\tau)^{1-\alpha} \cos(\pi\alpha/2)\right]}{1 + 2(\omega\tau)^{1-\alpha} \sin(\pi\alpha/2) + (\omega\tau)^{2(1-\alpha)}} \qquad (S5)$$

$$\chi'(\omega) = \chi_S + (\chi_T - \chi_S)\left(\frac{f_A\left[1 + (\omega\tau_A)^{1-\alpha_A} \sin(\pi\alpha_A/2)\right]}{1 + 2(\omega\tau_A)^{1-\alpha_A} \sin(\pi\alpha_A/2) + (\omega\tau_A)^{2(1-\alpha_A)}} + \frac{(1-f_A)\left[1 + (\omega\tau_B)^{1-\alpha_B} \sin(\pi\alpha_B/2)\right]}{1 + 2(\omega\tau_B)^{1-\alpha_B} \sin(\pi\alpha_B/2) + (\omega\tau_B)^{2(1-\alpha_B)}} \right) \qquad (S6)$$

$$\chi'(\omega) = (\chi_T - \chi_S)\left(\frac{f_A\left[1 + (\omega\tau_A)^{1-\alpha_A} \cos(\pi\alpha_A/2)\right]}{1 + 2(\omega\tau_A)^{1-\alpha_A} \sin(\pi\alpha_A/2) + (\omega\tau_A)^{2(1-\alpha_A)}} + \frac{(1-f_A)\left[1 + (\omega\tau_B)^{1-\alpha_B} \cos(\pi\alpha_B/2)\right]}{1 + 2(\omega\tau_B)^{1-\alpha_B} \sin(\pi\alpha_B/2) + (\omega\tau_B)^{2(1-\alpha_B)}} \right) \qquad (S7)$$

where χ_S is the adiabatic susceptibility, χ_T is the isothermal susceptibility, and τ is the average relaxation time of magnetization, and the α parameter, which ranges between

0 and 1, quantifies the width of the τ distribution, f_A represents the percentage of relaxation A.

References:

1. T. J. Atkins, J. E. Richman, W. F. Oettle, *Org. Synth.* **1978**, 58, 87

2. S.-S. Bao, L.-F. Ma, Y. Wang, L. Fang, C.-J. Zhu, Y.-Z. Li, L.-M. Zheng, *Chem.-Eur. J.* **2007**, 13, 2333-2343.

3. O. Kahn, *Molecular Magnetism*; VCH: New York, **1993**.

4. *SAINT, Program for Data Extraction and Reduction, Siemens Analytical X-ray instruments*, Madison, WI, 1994-1996.

5. *SHELXTL (version 5.0), Reference Manual, Siemens Industrial Automation, Analytical Instruments*, Madison, WI, 1995.

6. (a) H. Lueken, *Magnetochemie*, Teubner, Stuttart, Leipzig, **1999**. (b) H. Schilder, H. Lueken, *J. Magn. Magn. Mater.* **2004**, 281, 17.

7. B. G. Wybourne, *Spectroscopic Properties of Rare Earths*, Wiley, New York, **1965**.

8. D. Gatteschi, R. Sessoli, J. Villain, *Molecular Nanomagnets*, Oxford University, New York, **2006**.

9. N. Domingo, F. Luis, M. Nakano, M. Muntó, J. Gómez, J. Chaboy, N. Ventosa, J. Campo, J. Veciana, D. Ruiz-Molina, *Phys Rev B* **2009**, 79, 214404.

Table S1. Crystallographic data for compounds **1** - **2**.

Compound	1	2
Formula	$C_9H_{30}ErN_3O_{17}P_3$	$C_9H_{30}YN_3O_{17}P_3$
M	747.98	669.63
T/K	293(2)	296(2)
Crystal system	Triclinic	Triclinic
Space group	P-1	P-1
a /Å	9.0898(8)	9.133(5)
b /Å	9.1926(8)	9.226(5)
c /Å	15.1167(14)	15.198(8)
α/ deg	88.3976(12)	88.281(10)
β / deg	75.9926(10)	76.324(9)
γ / deg	75.8700(11)	75.787(9)
Z	2	2
V/Å^3	1187.84(18)	1205.7(11)
D_c / g·cm^{-3}	2.097	1.845
F(000)	742	684
Goodness-of-fit on F^2	1.001	1.053
R_1, wR$_2$[a] [I>2σ(I)]	0.0288, 0.0702	0.0655, 0.1764
R_1, wR$_2$ (all data)	0.0299, 0.0714	0.0831, 0.1909
$(\Delta\rho)_{max,}$, $(\Delta\rho)_{min}$/[e Å^{-3}]	1.597, -2.201	1.521, -1.618

$$ {}^{a}R_1 = \sum \left\| F_0 \right| - \left| F_c \right\| / \sum \left| F_0 \right|; \quad wR^2 \left[\sum w \left(F_0^2 - F_C^2 \right)^2 / \sum w \left(F_C^2 \right)^2 \right]^{1/2} $$

Table S2. Selected bond lengths [Å] for compounds **1**–**2**.

Compound	1	2		1	2
Ln1-O1	2.243(3)	2.238(5)	P1-O1	1.486(3)	1.488(5)
Ln1-O8C	2.201(3)	2.191(5)	P1-O3	1.581(3)	1.555(5)
Ln1-O4	2.410(3)	2.428(4)	P3-O7	1.509(3)	1.493(5)
Ln1-O6B	2.242(3)	2.246(4)	P3-O8	1.501(3)	1.508(5)
Ln1-O7	2.241(3)	2.253(5)	P3-O9	1.524(3)	1.522(5)
Ln1-O2A	2.288(3)	2.299(5)	P2-O6	1.498(3)	1.490(5)
Ln1-O1W	2.473(3)	2.475(5)	P2-O4	1.526(3)	1.528(5)
P1-O2	1.490(3)	1.472(5)	P2-O5	1.577(3)	1.561(5)

Symmetry transformations used to generate equivalent atoms: A: -x+1, -y, -z+1; B: -x, -y, -z+1; C: -x, -y+1, -z+1

Table S3. Selected bond angles [°] for compounds **1**–**2**.

Compound	1	2
O8C-Ln1-O6B	82.09(10)	81.42(18)
O8C-Ln1-O7	89.20(10)	87.62(18)
O6B-Ln1-O7	148.33(10)	147.04(17)
O8C-Ln1-O1	173.99(10)	172.65(17)
O6B-Ln1-O1	102.82(10)	104.62(18)
O7-Ln1-O1	84.81(10)	85.03(18)
O8C-Ln1-O2A	102.33(10)	103.78(18)
O6B-Ln1-O2A	75.42(10)	75.72(17)
O7-Ln1-O2A	136.25(10)	137.23(17)
O1-Ln1-O2A	82.41(10)	82.00(17)
O8C-Ln1-O4	97.62(10)	97.22(18)
O6B-Ln1-O4	76.52(9)	76.36(16)
O7-Ln1-O4	74.54(9)	74.31(16)
O1-Ln1-O4	80.36(10)	80.42(17)
O2A-Ln1-O4	142.69(10)	141.82(16)
O8C-Ln1-O1W	83.79(11)	83.75(19)
O6B-Ln1-O1W	136.90(10)	137.08(17)
O7-Ln1-O1W	71.40(10)	71.43(17)
O1-Ln1-O1W	94.69(10)	94.3(2)
O2A-Ln1-O1W	68.21(10)	69.14(18)
O4-Ln1-O1W	145.90(9)	145.67(16)

Symmetry transformations used to generate equivalent atoms: A: -x+1, -y, -z+1; B: -x, -y, -z+1; C: -x, -y+1, -z+1

Table S4. Geometry analysis of compounds **1** and **2** by SHAPE Software

Compound	Pentagonal bipyramid (D_{5h})	Capped octahedron (C_{3v})	Capped trigonal prism (C_{2v})
1	1.61448	3.85773	2.75697
2	1.79452	3.74169	2.52892

Table S5. CF Parameters determined for compound **1**.

Parameters	B_0^2 / cm^{-1}	B_0^4 / cm^{-1}	B_0^6 / cm^{-1}	SQX^a
1	-630.3	1661.0	-262.1	0.0045

a $SQX = \sqrt{\sum_{i=1}^{n} \left([\chi_{obs}(i) - \chi_{calc}(i)] / \chi_{obs}(i) \right)^2}$

Table S6. Energies and corresponding composition of the 8 doublets of the $^4I_{15/2}$ multiplets calculated with the CF parameters for compound **1**. Contributions lower than 1% are not shown here.

	M_J stark sublevel	Energy / cm^{-1}
1	$0.515 \pm|3/2> + 0.485 \pm|9/2>$	0
2	$0.637 \pm|11/2> + 0.336 \pm|5/2> + 0.027 \pm|1/2>$	10.58
3	$0.489 \pm|7/2> + 0.352 \pm|13/2> + 0.150 \pm|1/2>$	60.55
4	$0.805 \pm|13/2> + 0.195 \pm|7/2>$	90.54
5	$0.495 \pm|5/2> + 0.251 \pm|11/2> + 0.230 \pm|1/2> + 0.024 \pm|7/2>$	162.3
6	$\pm|15/2>$	173.0
7	$0.754 \pm|3/2> + 0.225 \pm|9/2>$	263.8
8	$0.422 \pm|1/2> + 0.369 \pm|5/2> + 0.200 \pm|7/2>$	326.4

Table S7. The parameters obtained by fitting the ac magnetic susceptibilities of compound **1** in indicated dc field at 1.8 K.

H / Oe	χ_T/ cm^3·mol^{-1}	χ_S/ cm^3·mol^{-1}	$\ln(\tau_A$ / s$)$	α_A	$\ln(\tau_B$ / s$)$	α_B	f_A	R^a
500	3.73	1.94	-3.83	0.22				2.6×10^{-5}
1000	3.59	1.07	-3.73	0.23				1.2×10^{-4}
1500	3.30	0.74	-4.65	0.20	-2.31	0.00	0.67	2.0×10^{-4}
2000	3.01	0.56	-5.43	0.18	-2.28	0.00	0.53	1.7×10^{-4}
2500	2.82	0.45	-6.06	0.20	-2.08	0.05	0.40	2.0×10^{-4}
3000	2.44	0.37	-6.58	0.25	-2.02	0.03	0.38	2.7×10^{-4}

a $R = \sum \left[(\chi'_{obs} - \chi'_{cal})^2 + (\chi''_{obs} - \chi''_{cal})^2 \right] / \sum \left[\chi'^2_{obs} + \chi''^2_{obs} \right]$

Table S8. The parameters obtained by fitting the ac magnetic susceptibilities of compound **1** under 1 kOe dc field.

T / K	χ_T/ cm^3·mol^{-1}	χ_S/ cm^3·mol^{-1}	$\ln(\tau/\text{s})$	α	R^a
1.8	3.61	1.06	-3.71	0.24	7.2×10^{-5}
2.0	3.46	1.02	-3.96	0.24	3.2×10^{-5}
2.3	3.01	0.92	-4.68	0.22	6.3×10^{-5}
2.5	2.74	0.84	-5.50	0.21	2.4×10^{-4}
2.7	2.52	0.78	-6.45	0.18	4.0×10^{-4}
3.0	2.21	0.71	-7.92	0.12	7.1×10^{-5}
3.2	2.08	0.61	-8.86	0.12	2.1×10^{-5}
3.4	1.97	0.80	-9.37	0.07	3.7×10^{-5}
3.6	1.89	0.88	-9.97	0.10	3.1×10^{-5}
3.8	1.82	1.07	-10.40	0.15	2.0×10^{-5}

a $R = \sum \left[(\chi'_{obs} - \chi'_{cal})^2 + (\chi''_{obs} - \chi''_{cal})^2 \right] / \sum \left[\chi'^2_{obs} + \chi''^2_{obs} \right]$

Table S9. The parameters obtained by fitting the ac magnetic susceptibilities of compound **1** under 2 kOe dc field.

T / K	χ_T/ cm^3·mol^{-1}	χ_S/ cm^3·mol^{-1}	$\ln(\tau_A/\text{s})$	α_A	$\ln(\tau_B/\text{s})$	α_B	f_A	R^a
1.8	3.01	0.56	-5.43	0.18	-2.28	0.10	0.52	1.7×10^{-4}
2.0	3.12	0.55	-5.60	0.16	-2.37	0.10	0.46	4.5×10^{-5}
2.3	2.78	0.52	-5.78	0.16	-2.70	0.09	0.55	4.2×10^{-5}
2.5	2.71	0.49	-6.13	0.16	-2.72	0.21	0.57	2.6×10^{-4}
2.7	2.52	0.47	-6.79	0.13	-3.09	0.25	0.58	8.2×10^{-6}
3.0	2.34	0.45	-7.96	0.09	-3.57	0.40	0.58	1.1×10^{-5}
3.2	2.18	0.42	-8.71	0.10	-3.82	0.36	0.65	1.9×10^{-5}
3.4	2.08	0.57	-9.19	0.04	-4.04	0.40	0.63	2.5×10^{-5}
3.6	2.00	0.64	-9.69	0.10	-4.23	0.44	0.62	1.8×10^{-5}
3.8	1.88	0.77	-10.09	0.04	-4.37	0.41	0.65	1.2×10^{-5}

a $R = \sum \left[(\chi'_{obs} - \chi'_{cal})^2 + (\chi''_{obs} - \chi''_{cal})^2 \right] / \sum \left[\chi'^2_{obs} + \chi''^2_{obs} \right]$

Table S10. The parameters obtained by fitting the ac magnetic susceptibilities of compound **1a** in indicated dc field at 1.8 K.

H / Oe	χ_T/ cm^3·mol^{-1}	χ_S/ cm^3·mol^{-1}	ln(τ/ s)	α	R^a
500	3.50	1.22	-6.57	0.09	2.2×10^{-5}
1000	3.35	0.69	-6.35	0.10	8.5×10^{-4}
1500	3.14	0.41	-6.36	0.12	2.2×10^{-4}
2000	2.70	0.28	-6.62	0.17	6.5×10^{-4}
2500	2.65	0.24	-6.66	0.20	9.0×10^{-4}
3000	2.39	0.22	-6.93	0.22	1.5×10^{-4}

$a\,R = \sum \left[(\chi'_{obs} - \chi'_{cal})^2 + (\chi''_{obs} - \chi''_{cal})^2 \right] / \sum \left[{\chi'_{obs}}^2 + {\chi''_{obs}}^2 \right]$

Table S11. The parameters obtained by fitting the *ac* magnetic susceptibilities of compound **1a** under 1 kOe *dc* field.

T / K	χ_T/ cm^3·mol^{-1}	χ_S/ cm^3·mol^{-1}	ln(τ/ s)	α	R^a
1.8	3.35	0.69	-6.35	0.10	8.5×10^{-4}
2.0	3.06	0.70	-6.71	0.10	7.0×10^{-4}
2.3	2.72	0.78	-7.31	0.11	4.4×10^{-4}
2.5	2.53	0.91	-7.66	0.13	2.5×10^{-4}
2.7	2.37	1.09	-7.88	0.14	1.3×10^{-4}
3.0	2.17	1.27	-8.20	0.18	1.4×10^{-4}
3.2	2.06	1.36	-8.37	0.24	1.5×10^{-4}
3.4	1.95	1.44	-8.56	0.29	1.9×10^{-4}
3.6	1.84	1.65	-7.59	0.02	1.1×10^{-4}

$a\,R = \sum \left[(\chi'_{obs} - \chi'_{cal})^2 + (\chi''_{obs} - \chi''_{cal})^2 \right] / \sum \left[{\chi'_{obs}}^2 + {\chi''_{obs}}^2 \right]$

Table S12. The parameters obtained by fitting the ac magnetic susceptibilities of compound **1a** under 2 kOe dc field.

T / K	χ_T/ cm^3·mol^{-1}	χ_S/ cm^3·mol^{-1}	ln(τ/ s)	α	R^a
1.8	2.70	0.28	-6.62	0.17	6.5×10^{-4}
2.0	2.74	0.32	-6.71	0.18	4.5×10^{-4}
2.3	2.52	0.34	-7.23	0.23	3.0×10^{-4}
2.5	2.36	0.42	-7.59	0.25	1.3×10^{-4}
2.7	2.23	0.54	-7.87	0.26	1.2×10^{-4}
3.0	2.06	0.73	-8.23	0.26	3.9×10^{-5}
3.2	1.95	0.85	-8.44	0.26	5.2×10^{-5}
3.4	1.86	1.07	-8.62	0.21	4.6×10^{-5}
3.6	1.78	1.09	-8.77	0.25	3.4×10^{-5}

$a\,R = \sum \left[(\chi'_{obs} - \chi'_{cal})^2 + (\chi''_{obs} - \chi''_{cal})^2 \right] / \sum \left[{\chi'_{obs}}^2 + {\chi''_{obs}}^2 \right]$

Table S13. Energy peak position and full-width-at-half maximum (*fwhm*) of the $^4I_{13/2}$, $^4I_{15/2}$ Stark components determined from the experimental emission spectrum (acquired at 300 K) best fit ($\chi^2_{red} = 1.5\times10^{-6}$) using a 10-components Gaussian function for **1**.

Line	Energy / cm^{-1}	*fwhm* / cm^{-1}
1[a]	6638.8 ± 2.0	61.0 ± 2.7
2	6514.6 ± 3.5	88.0 ± 3.9
3[a]	6509.5 ± 0.8	21.1 ± 1.3
4	6478.4 ± 2.1	30.7 ± 4.0
5	6455.3 ± 0.3	14.9 ± 0.9
6	6433.5 ± 0.4	37.0 ± 2.9
7	6401.6 ± 0.3	21.2 ± 0.8
8	6377.6 ± 0.6	26.3 ± 2.7
9	6360.0 ± 17	40.3 ± 12
10	6322.2 ± 7.7	115.2 ± 6.9

a: hot band
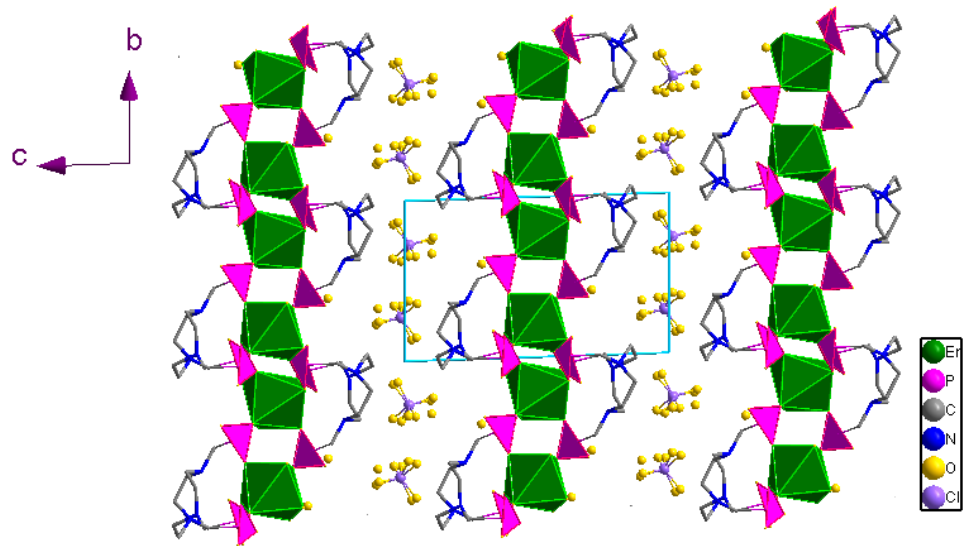
Figure S1. Packing diagram of structure **1** along the *a*-axis.
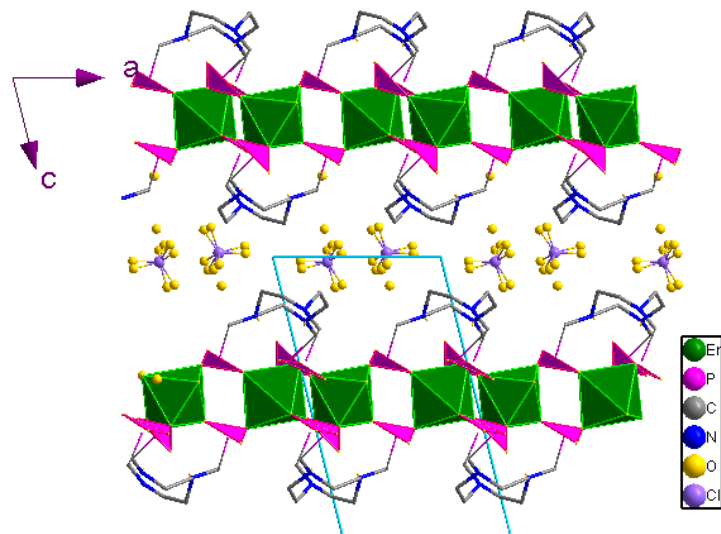
Figure S2. Packing diagram of structure **1** along the *b*-axis.
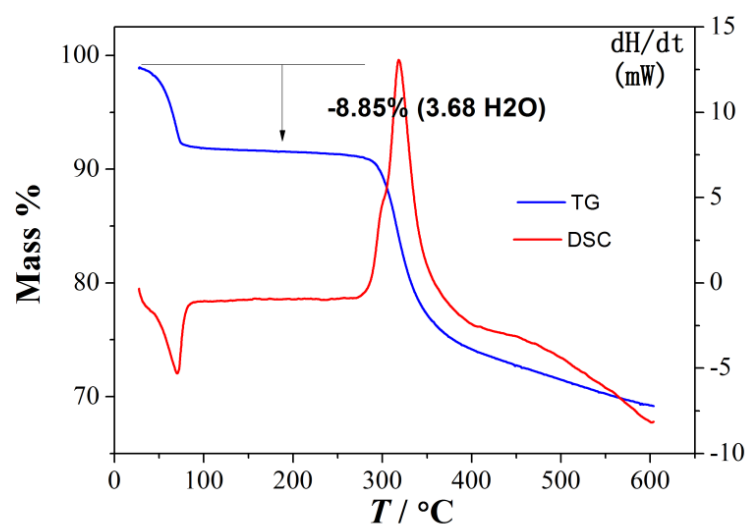
Figure S3. TG analysis of compound **1**.
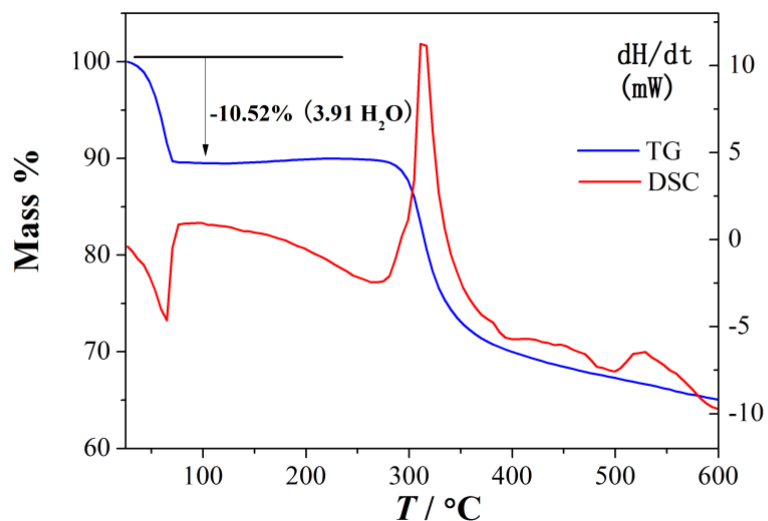
Figure S4. TG analysis of compound **2**.
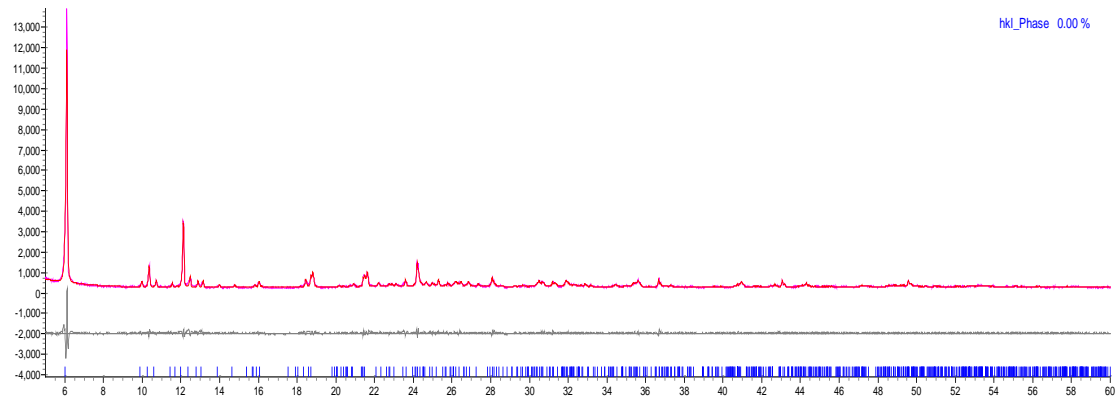
Figure S5. PXRD pattern of **1** refined by *TOPAS* software. *Rwp* = 8.76%. Cell parameters: *P*-1, a = 9.159 Å, b = 9.247 Å, c = 15.160 Å, α = 87.934°, β = 76.555°, γ = 75.622°, V = 1209.4 Å^3
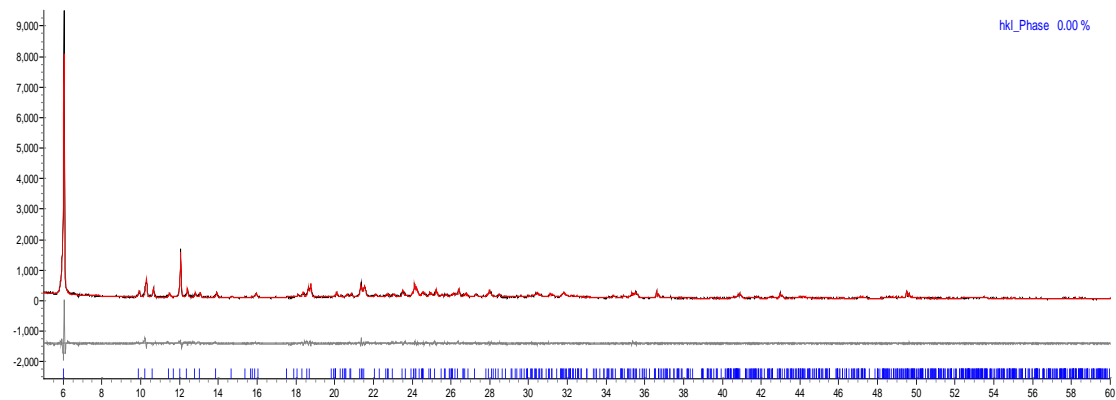
Figure S6. PXRD pattern of **2** refined by *TOPAS* software. *Rwp* = 11.89%. Cell parameters: *P*-1, a = 9.168 Å, b = 9.244 Å, c = 15.159 Å , α = 87.928°, β = 76.523°, γ = 75.696°, V = 1210.3 Å^3.
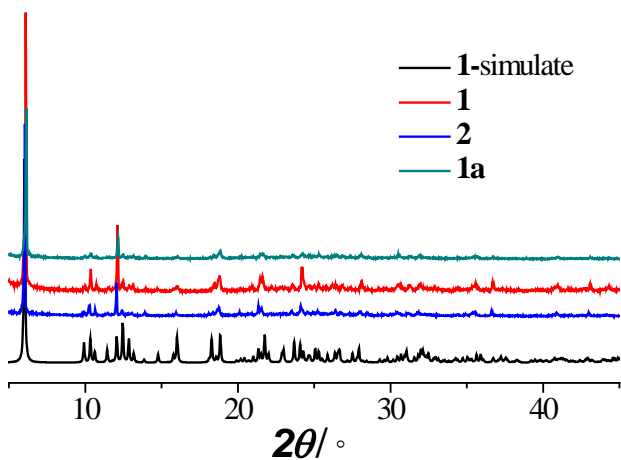
Figure S7. PXRD patterns for compounds **1**, **2** and **1a**.
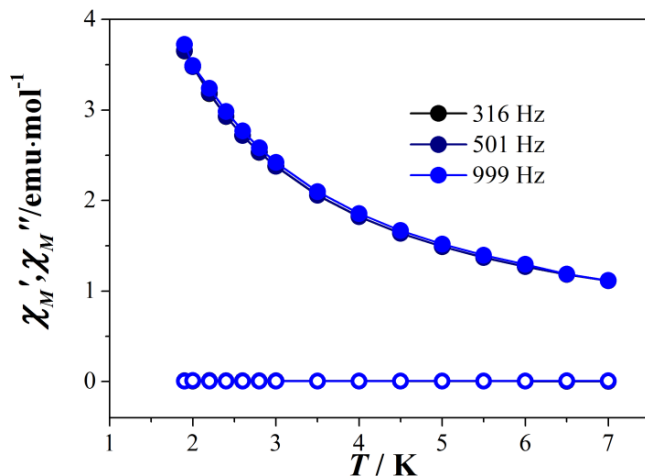
Figure S8. Temperature dependent in-phase (χ_M') and out-of-phase (χ_M'') signals of **1** in zero dc field.
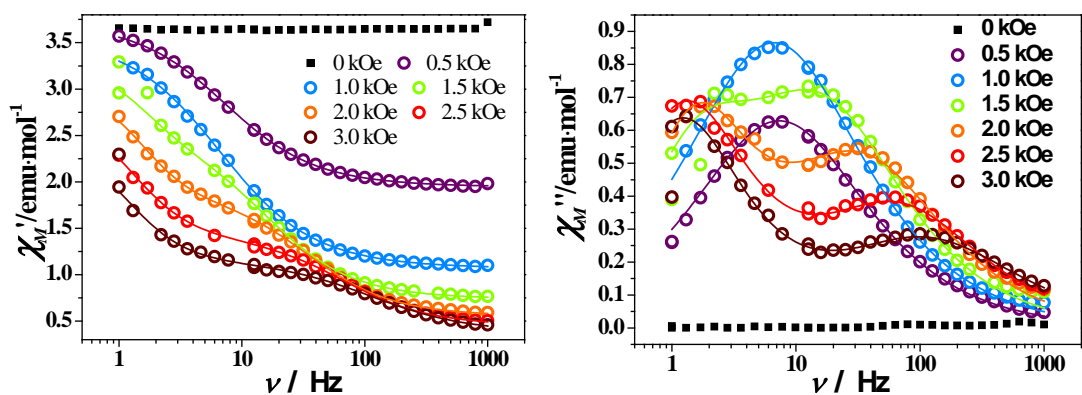
Figure S9. Frequency dependent in-phase (χ_M') and out-of-phase (χ_M'') signals of **1** in indicated dc fields at 1.8 K. The solid lines represent the simulated results.
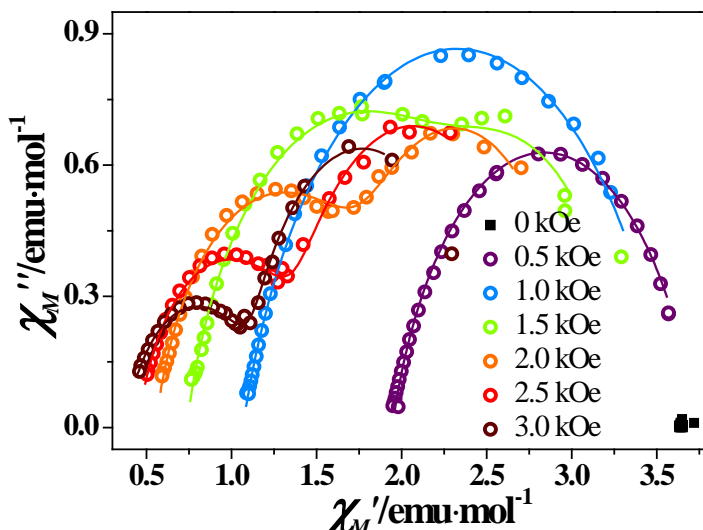
Figure S10. Cole-Cole plots of **1** in indicated dc fields at 1.8 K. The solid lines represent the simulated results.
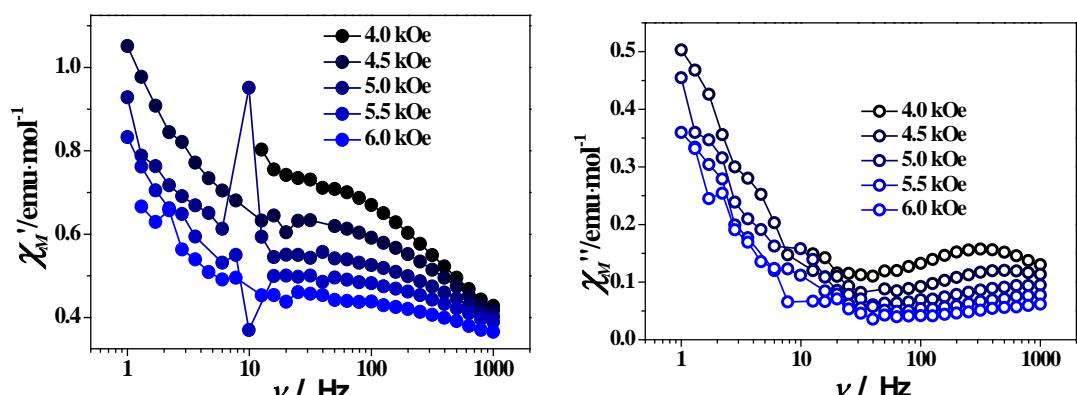
**Figure S11**. Frequency dependent in-phase ($\chi_M{}'$) and out-of-phase ($\chi_M{}''$) signals of **1** in indicated high dc fields at 1.8 K.
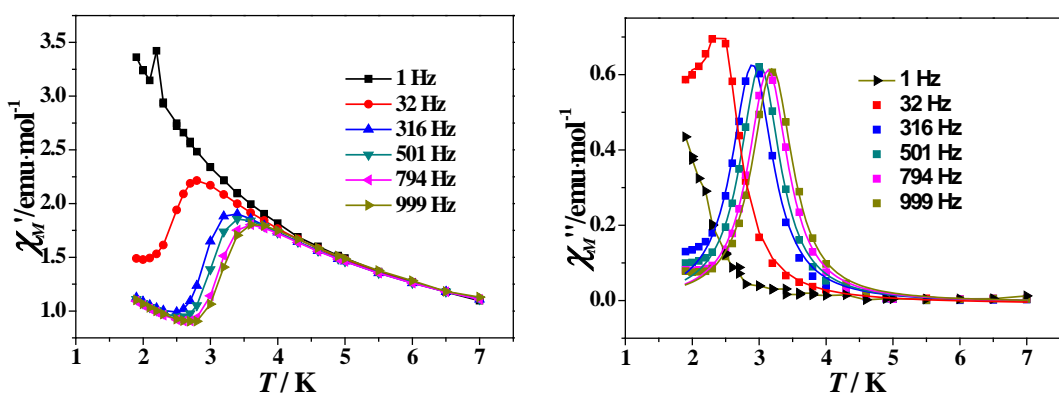
Figure S12. Temperature dependent in-phase ($\chi_M{}'$) and out-of-phase ($\chi_M{}''$) signals of **1** in 1 kOe dc field.
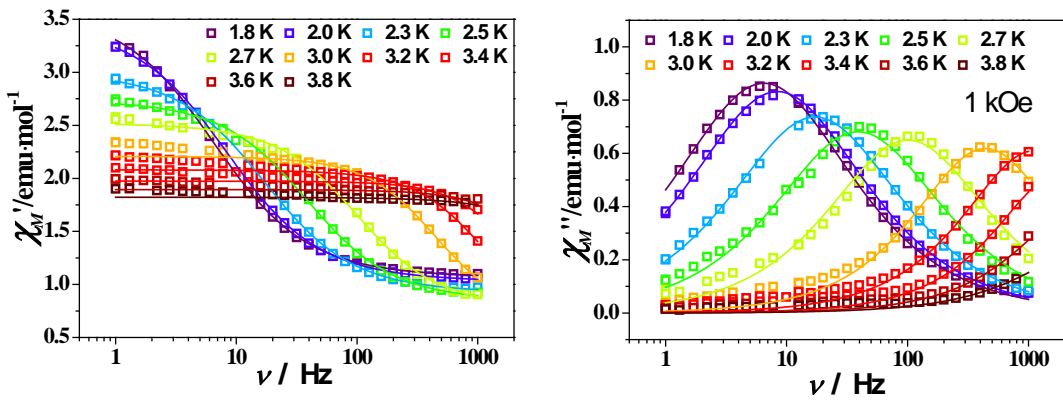
Figure S13. Frequency dependent in-phase (χ_M') and out-of-phase (χ_M'') signals of **1** in 1 kOe dc field. The solid lines represent the simulated results.
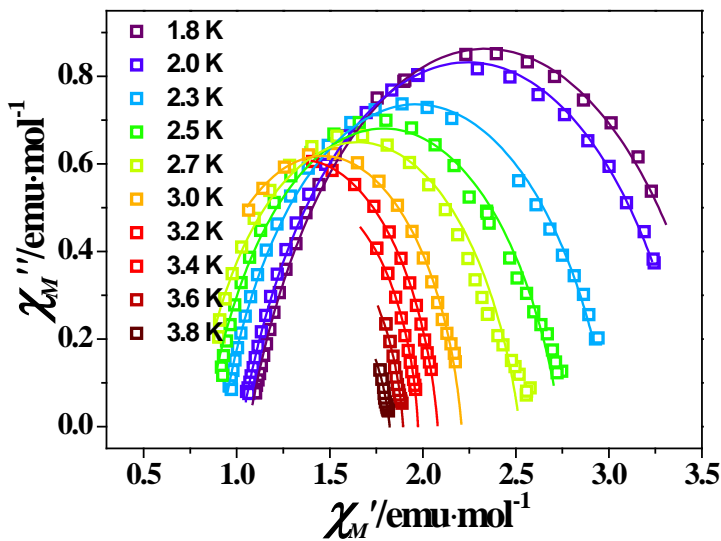

Figure S14. Cole-Cole plots of **1** in the1 kOe dc field. The solid lines represent the simulated results.
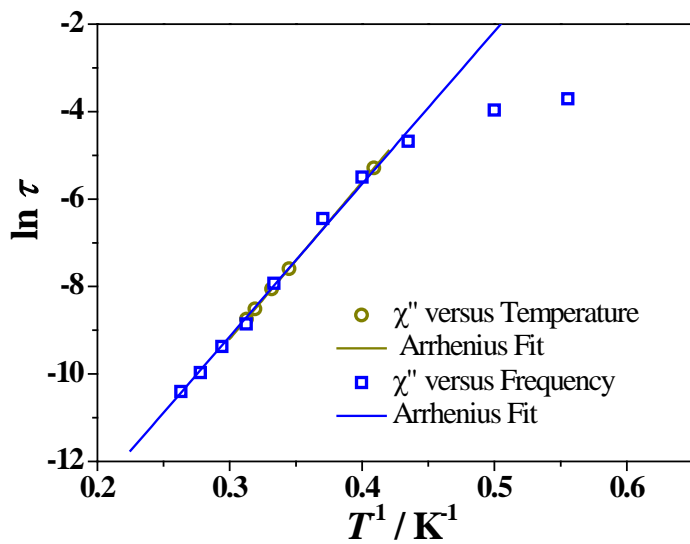
Figure S15. Magnetization relaxation time (τ) versus T^{-1} plots for **1** in 1 kOe dc field.
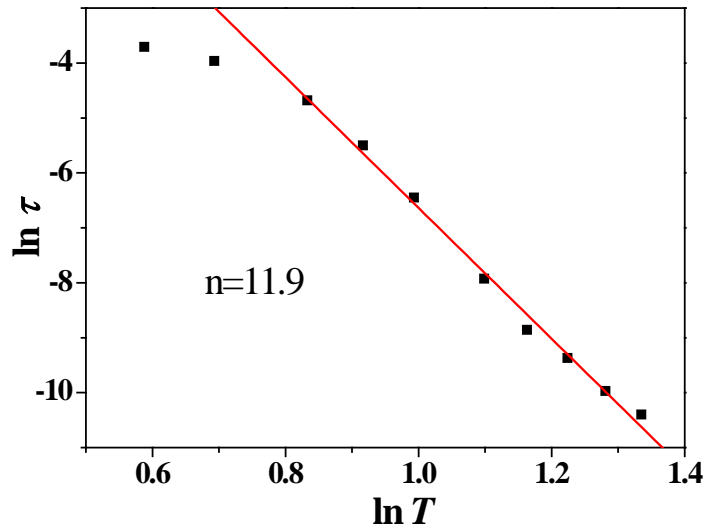
Figure S16. The relaxation time of **1** in 1 kOe dc field fitted with $\ln \tau = -n \cdot \ln T$ in the high temperature region. The resulted value of n = 11.9 (larger than 9) rules out the Raman relaxation process.
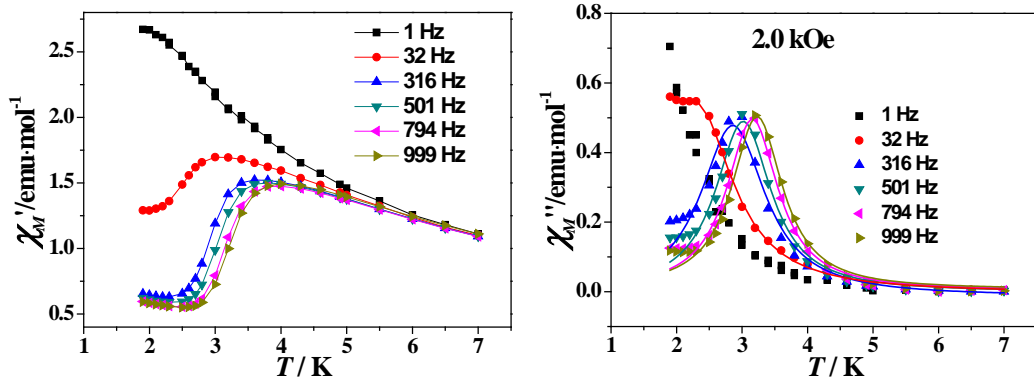
Figure S17. Temperature dependent in-phase (χ_M') and out-of-phase (χ_M'') signals of **1** in 2 kOe dc field.
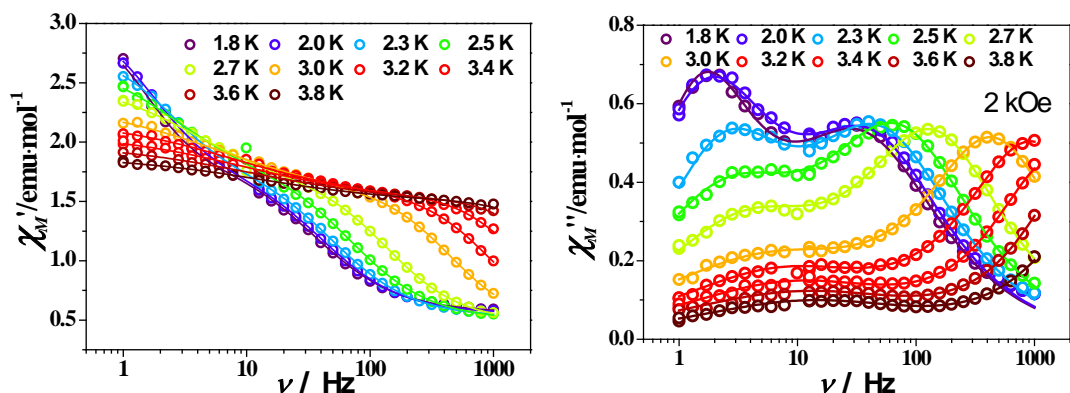
Figure S18. Frequency dependent in-phase (χ_M') and out-of-phase (χ_M'') signals of **1** in 2 kOe dc field. The solid lines represent the simulated results.
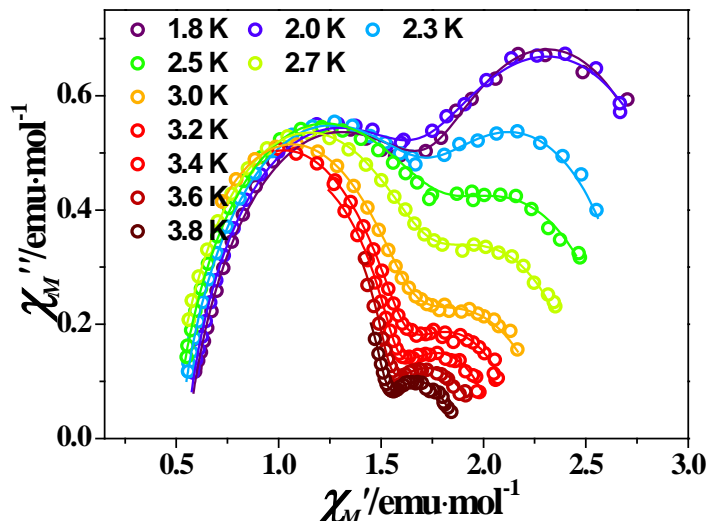
**Figure S19**. Cole-Cole plots of **1** in 2 kOe dc field. The solid lines represent the simulated results.
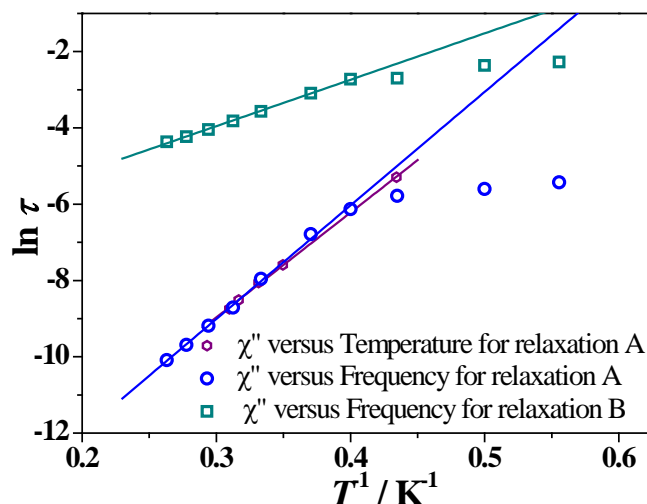
Figure S20. Magnetization relaxation time (τ) versus T^{-1} plots for **1** in 2 kOe dc field.
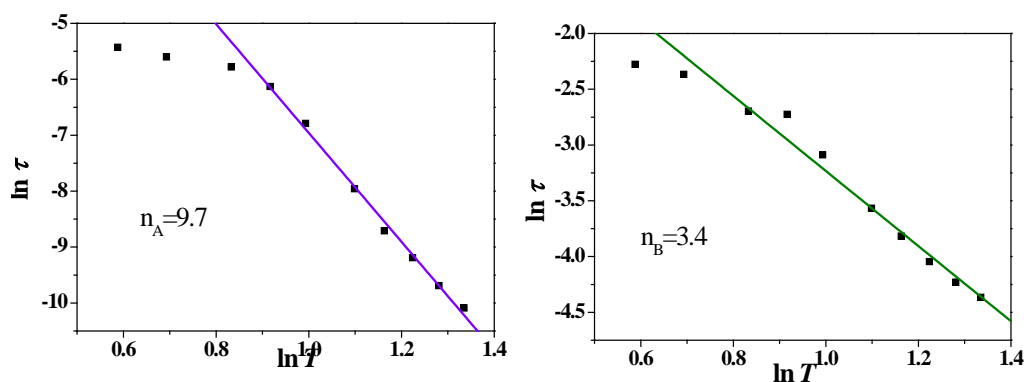
Figure S21. The relaxation times of **1** at 2 kOe dc field are fitted with equation: $\ln \tau = -n \cdot \ln T$. For relaxation A, $n = 9.7$ (larger than 9) which rules out the Raman relaxation process; for relaxation B, $n = 3.4$ which falls in the region of $n = 1 – 6$ expected for Raman-like process.
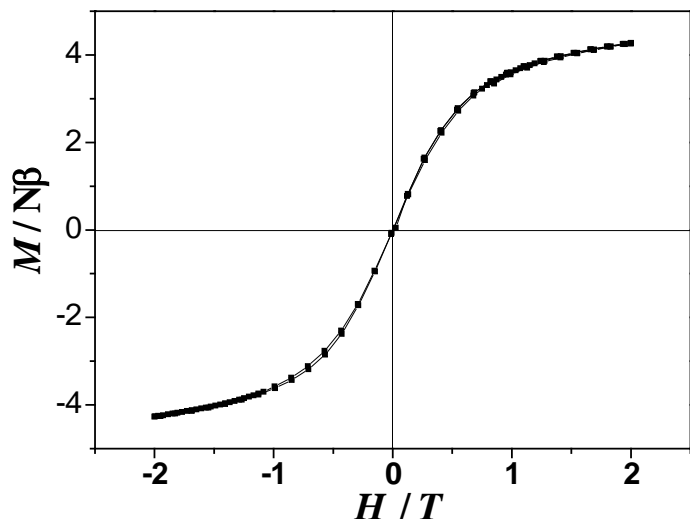
Figure S22. *M vs. H* plot for **1** at 1.9 K.
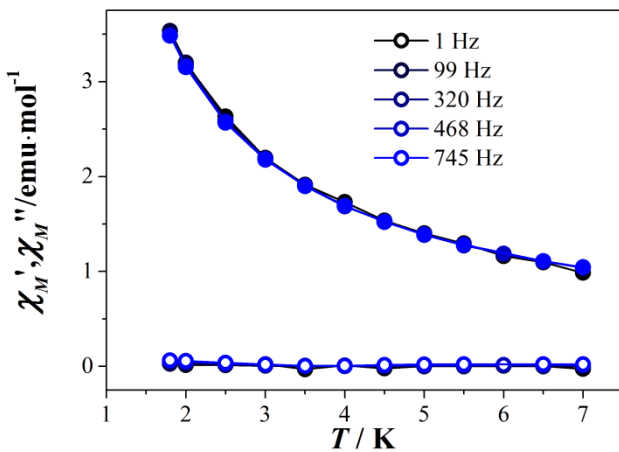
Figure S23. Temperature dependent in-phase (χ_M') and out-of-phase (χ_M'') signals of **1a** in zero field.
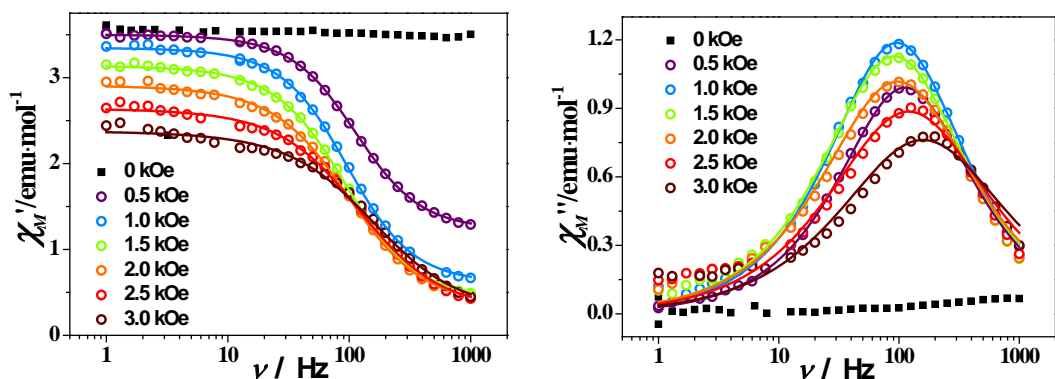
Figure S24. Frequency dependent in-phase (χ_M') and out-of-phase (χ_M'') signals of **1a** in indicated dc fields at 1.8 K. The solid lines represent the simulated results.
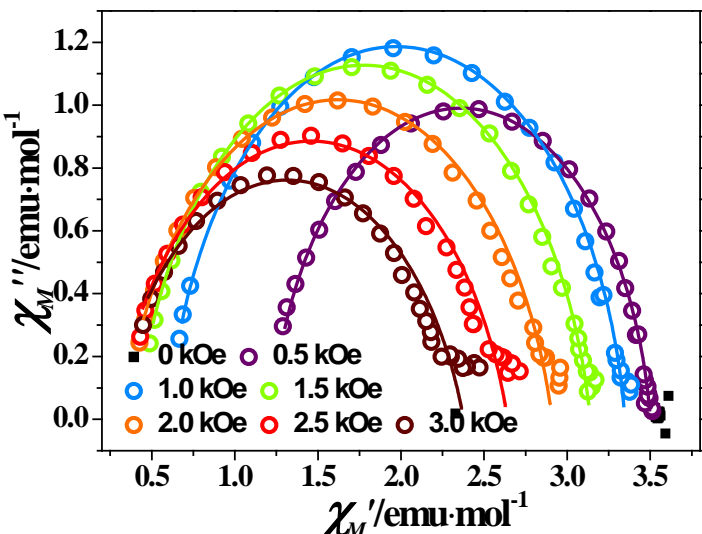
Figure S25. Cole-Cole plots of **1a** in the 2 kOe dc field. The solid lines represent the simulated results.
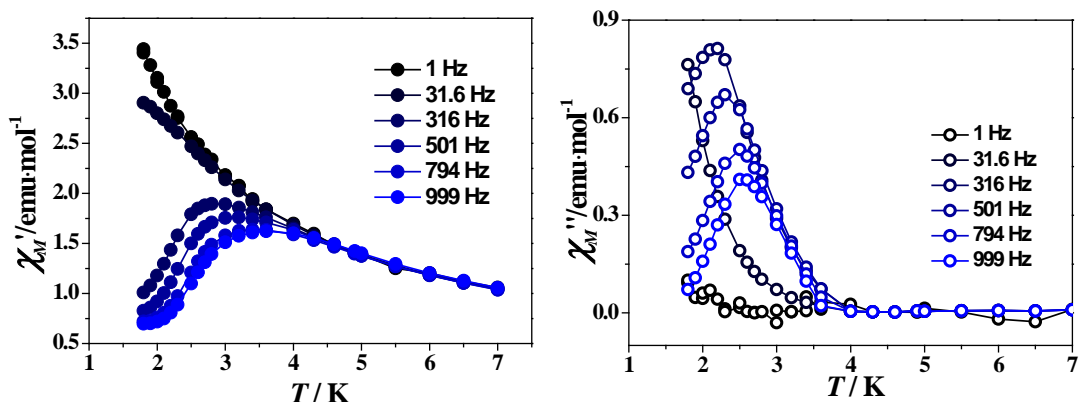

Figure S26. Temperature dependent in-phase (χ_M') and out-of-phase (χ_M'') signals of **1a** in 1 kOe dc field.
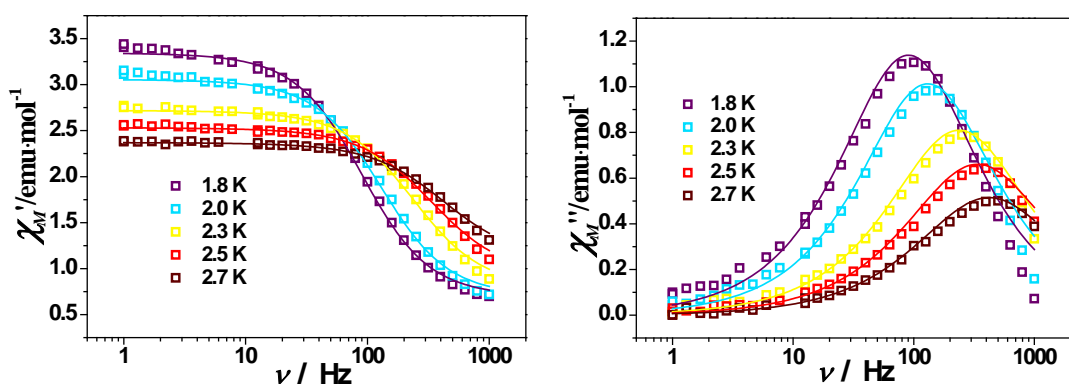

Figure S27. Frequency dependent in-phase (χ_M') and out-of-phase (χ_M'') signals of **1a** in 1 kOe dc field. The solid lines represent the simulated results.
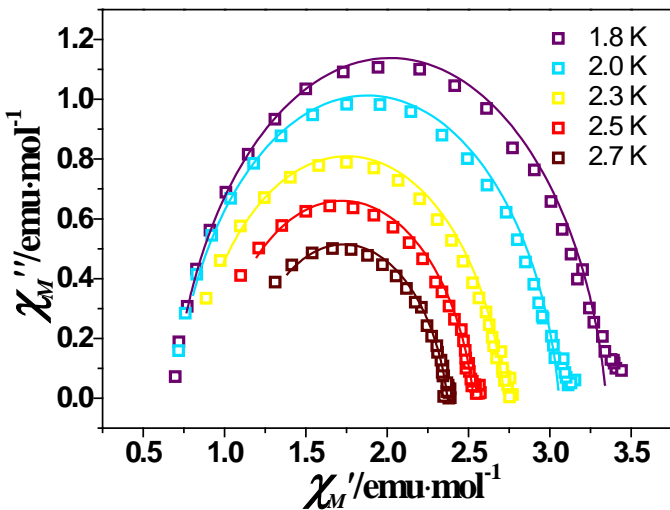
Figure S28. Cole-Cole plots of **1a** in the 1 kOe dc field. The solid lines represent the simulated results.
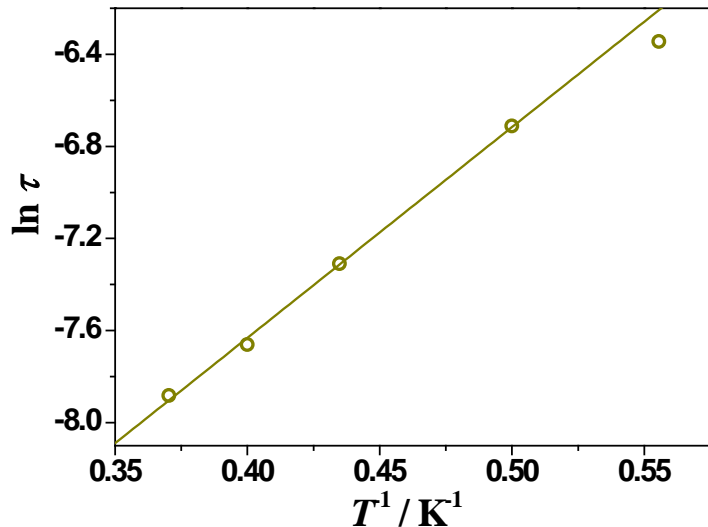
Figure S29. The lnτ vs. T^{-1} plots of **1a** in 1 kOe *dc* field. The solid lines are best fits according to the Arrhenius law: U = 9.2 K ($\tau_0 = 1.24 \times 10^{-5}$ s).
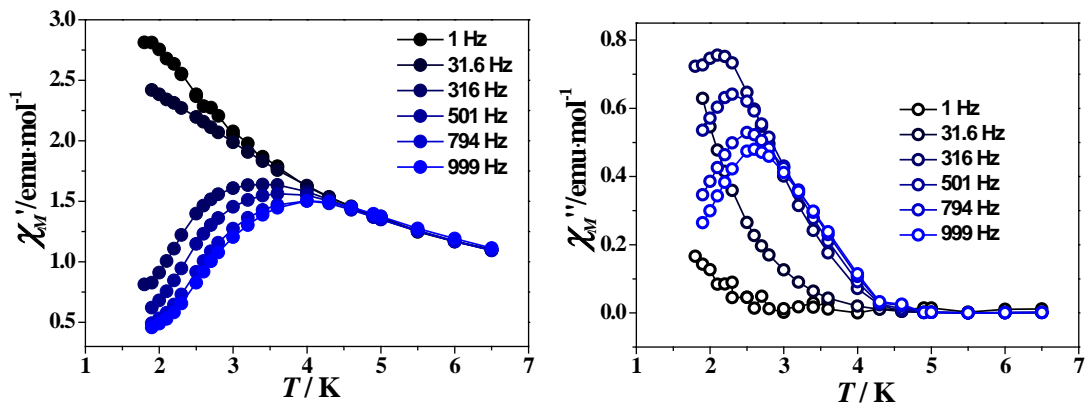
Figure S30. Temperature dependent in-phase (χ_M') and out-of-phase (χ_M'') signals of **1a** in 2 kOe dc field.
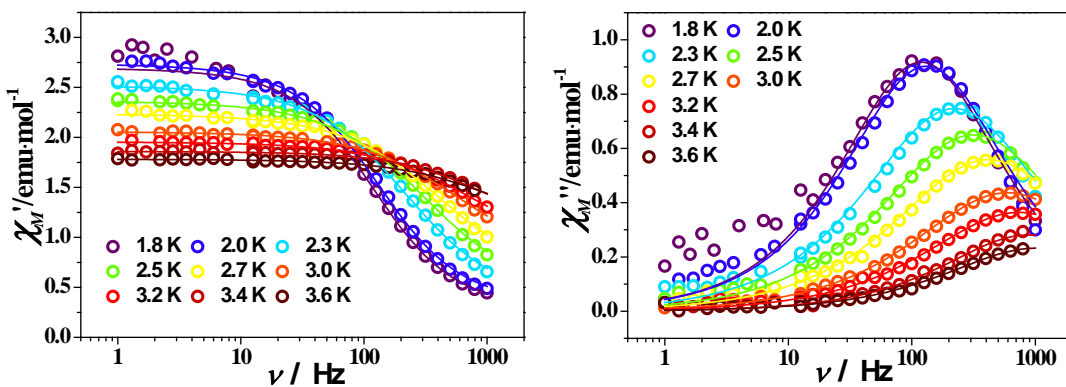
Figure S31. Frequency dependent in-phase (χ_M') and out-of-phase (χ_M'') signals of **1a** in 2 kOe dc field. The solid lines represent the simulated results.
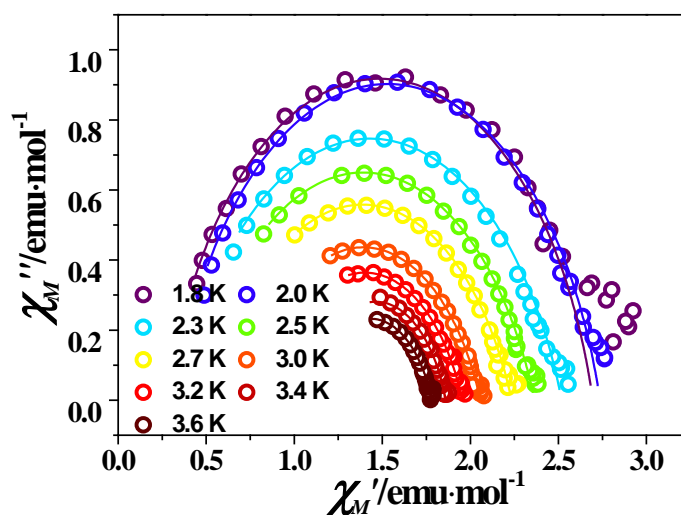

Figure S32. Cole-Cole plots of **1a** in the 2 kOe dc field. The solid lines represent the simulated results.
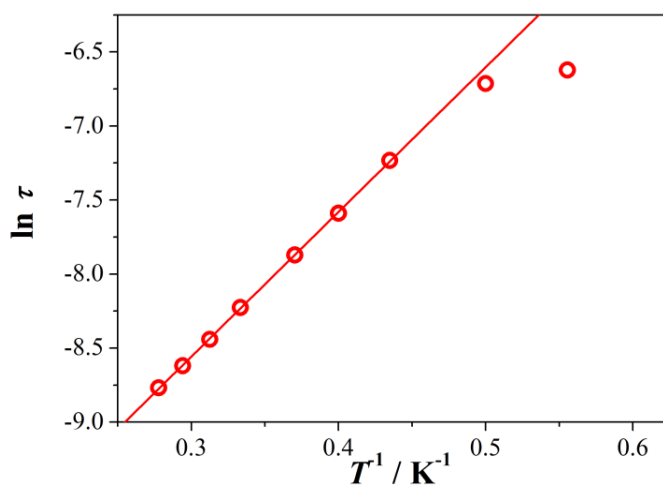

Figure S33. Magnetization relaxation time (τ) vs. T^{-1} plot for **1a** in 2 kOe dc field. The solid line represents the best fit according to the Arrhenius law.
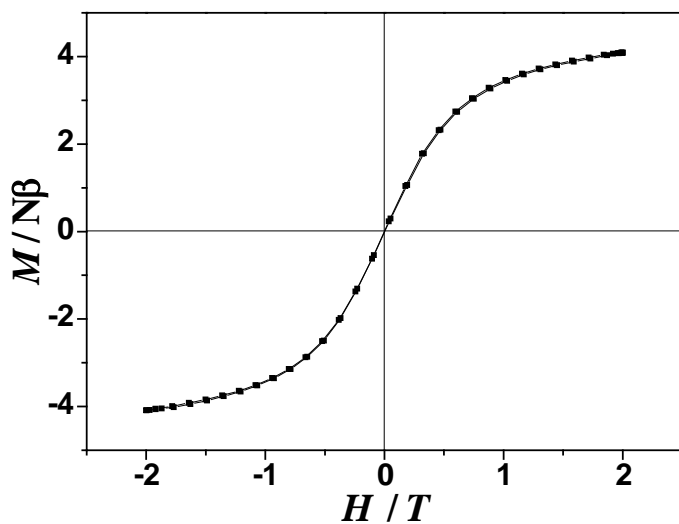
**Figure S34**. The *M vs. H* plot for **1a** at 1.8 K.
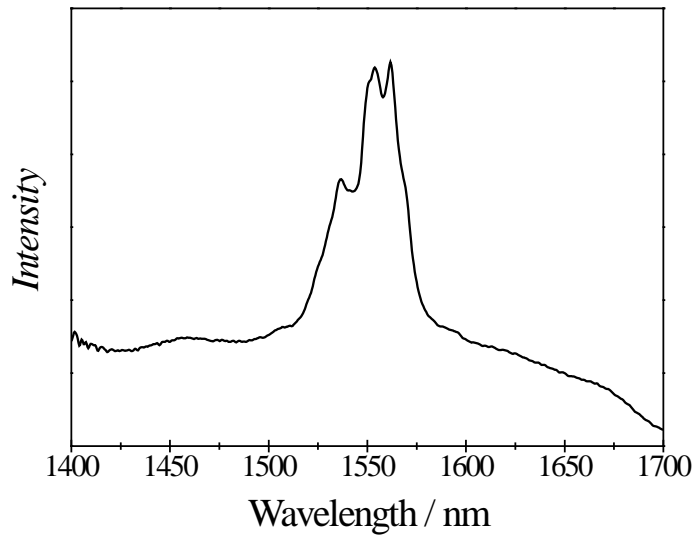
Figure S35. The NIR emission spectrum of **1** excited at Nd:YAG laser at room temperature.